J Eng Math (2018) 113:23–43
https://doi.org/10.1007/s10665-018-9972-8

Modeling coating flow and surfactant dynamics inside the alveolar compartment

D. Kang · M. Chugunova · A. Nadim · A. J. Waring · F. J. Walther

Received: 5 February 2018 / Accepted: 3 September 2018 / Published online: 20 September 2018

Abstract We derive a new model for the coating flow inside the alveolar compartment, taking into account pulmonary surfactant production and recycling by Type 2 cells as well as its degradation. As the thickness of alveolar coating is much smaller than the average radius of the alveoli, we employ the classical lubrication approximation to describe the thin liquid film dynamics in the presence of pulmonary surfactant, which is a surface tension-reducing agent and thus prevents the lungs from collapse. In the lubrication limit, we derive a degenerate system of two coupled parabolic partial differential equations that describe the time evolution of the thickness of the coating film inside the alveoli together with that of the surfactant concentration at the interface. We present numerical simulations using parameter values consistent with experimental measurements. With Marangoni effects being significant, it is found that any initial non-uniformity in surfactant concentration leads to a very fast redistribution of surfactant and accompanying change in film thickness, followed by a much slower relaxation of the film thickness to equilibrium during which surfactant concentration remains relatively uniform.

Keywords Alveolar modeling · Lubrication approximation · Scientific computations · Surface tension · Surfactant · Thin liquid film

D. Kang · M. Chugunova · A. Nadim (✉)
Institute of Mathematical Sciences, Claremont Graduate University, Claremont, CA 91711, USA
e-mail: ali.nadim@cgu.edu

D. Kang
e-mail: di.kang@cgu.edu

M. Chugunova
e-mail: marina.chugunova@cgu.edu

A. J. Waring · F. J. Walther
Los Angeles Biomedical Research Institute, Harbor-University of California at Los Angeles (UCLA) Medical Center, Torrance, CA 90502, USA
e-mail: awaring@labiomed.org

F. J. Walther
e-mail: fwalther@labiomed.org

1 Introduction

Oxygen exchange in the lungs occurs across the membranes of small balloon-like structures called alveoli attached to the branches of the bronchial passages. These alveoli inflate and deflate with inhalation and exhalation. The behavior of the alveoli is largely dictated by Laplace's law (that describes the pressure difference across an interface in fluid mechanics) involving surface tension. It takes some effort to breathe in because these tiny balloons must be inflated, but the elastic recoil of the tiny balloons assists us in this process. Inflating the alveoli in the process of respiration requires an excess pressure inside the alveoli relative to their surroundings. This is accomplished by making the pressure in the thoracic cavity negative with respect to atmospheric pressure. The amount of net pressure required for inflation is dictated by the surface tension and radii of the tiny balloon-like alveoli. During inhalation the radii of the alveoli increase from about 0.05 to 0.1 mm. The alveolar lining fluid (the alveolar hypophase, without surfactant) has a nominal surface tension of about 50 dyn/cm so the required net outward pressure is about $\Delta P = 15$ mmHg when $r = 0.05$ mm and $\Delta P = 7.5$ mmHg when $r = 0.1$ mm, but the actual normal pressure difference in respiration is only about 1 mmHg [2].

A remarkable property of lung surfactant, which coats the alveoli, is that it reduces the surface tension by a factor of about 15 so that a 1 mmHg pressure differential is sufficient to inflate the alveoli. There appears to be a nearly constant amount of this surfactant per alveolus, so that when the alveoli are deflated, it is more concentrated on the surface. Since the surface-tension-lowering effect of surfactant depends on this concentration, it diminishes the required pressure for inflation of the alveoli at their most critical phase. For a given surface tension, the pressure to inflate a smaller bubble is greater. It is the surfactant which makes it possible to inflate the alveoli with only about 1 mmHg of excess pressure over the surroundings. Because neighboring alveoli communicate with each other via alveolar pores (pores of Kohn connect alveoli to adjacent alveoli), their surface tensions must be different (if they are different in size) in order to prevent the collapse of small alveoli in favor of large ones. Mechanical coupling of alveoli via the interstitial tissue is an additional mechanism that prevents alveolar collapse [3].

The lung is very sensitive to gravity, and it is of current interest to know how its function is altered in the weightlessness of space. For example, studies on NASA Spacelabs [4] show an unexpectedly large increase in the diffusing capacity of the alveolar membrane due to uniform alveolar expansion. Effect of microgravity on pulmonary surfactant properties was studied in [5]. The properties of pulmonary surfactant were assessed by the evaluation of surface activity (surface tension), and the experiments indicated that there was roughly a 50% decrease in surface activity of pulmonary surfactant films after some time in the microgravity environment.

The epithelium lining the walls of the alveoli is composed primarily of large, squamous Type 1 cells and smaller, granular, and roughly cuboidal Type 2 cells (see Fig. 1). The alveolar Type 1 cell (volume 1800 μm^3) is an important

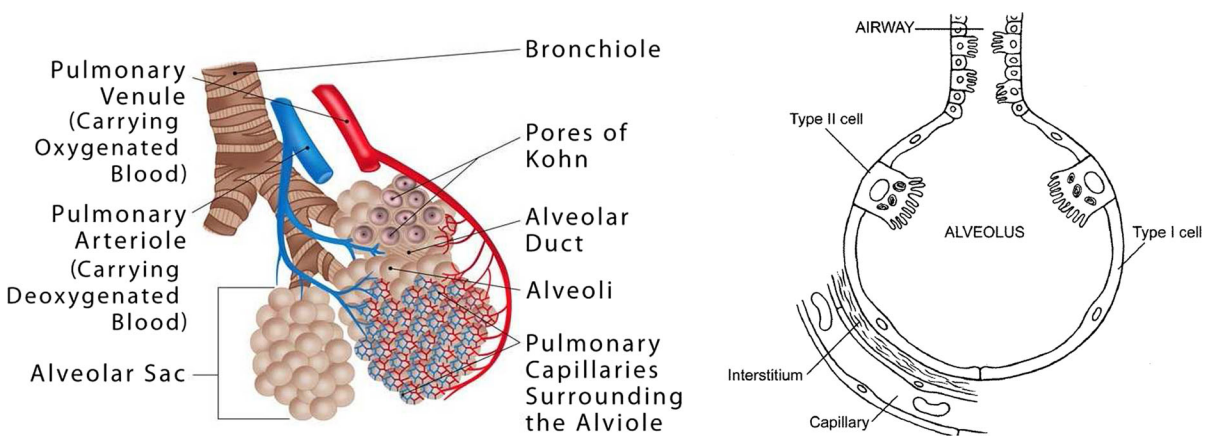

Fig. 1 Alveolar sac schematic on the left (adapted from www.therespiratorysystem.com) and cell types present in alveolar compartment on the right (adapted from [1])

component of the air–blood barrier, as it overlies capillaries in the alveolar wall and comprises most (90%) of its surface area. This has been described in papers about proteins that are predominantly expressed by Type 1 cells in the lungs, such as the plasma membrane protein T1-a [6] and aquaporins, a family of water channels [7]. Although Type 2 cells (volume 900 μm^3 and thickness 0.2 μm) occupy only 10% of the alveolar surface area, there are about twice as many of them (60% of alveolar epithelial cells are Type 2) as Type 1 cells [8,9]. At the same time, Type 2 cells comprise only 15% of peripheral lung cells; they are typically found at the alveolar–capillary barrier, and they have an apical surface area of about 250 μm^2 per cell [3]. Alveolar surfactant has a half life of about 24 h, once secreted, depending on maturity/illness according to studies with stable isotopes [10]. Viscosity values for some clinical animal-derived lung surfactants are presented in Table 1 of [11]. One of the major functions of the Type 2 cells is the synthesis and secretion of surfactant. Cryoscanning electron microscopy of frozen tissue demonstrated surfactant to cover extended areas of alveolar surface as a continuous, thin layer [12]. Approximately 90% of the surfactant is recycled from the alveolar space back into the same Type 2 cells [13]. Type 2 cells are called defenders of the alveolar epithelium because they proliferate to restore Type 1 cells after lung damage. Alveolar Type 1 and 2 cells transport sodium to keep the alveolus relatively free from fluid, and participate in innate immunity to fight infection. While not specific to the alveoli, a mathematical model for the regulation of fluid in the airways has been developed in [14].

The baby's first breath depends a lot upon the presence of pulmonary surfactant and is made more difficult in premature infants by the incomplete formation of this surface-tension-reducing agent. Approximately 7% of all infants are born prematurely, and half of them develop respiratory distress syndrome due to lack of the surfactant. Aerosol delivery of synthetic lung surfactant is being investigated as a new technique of respiratory support for such babies [15] and as a potential replacement for the widely used intratracheal delivery of animal-derived surfactant. One of the objectives of our research is to better understand the required properties of substitute synthetic surfactant through mathematical modeling of lung surfactant dynamics.

Biomedical applications of surfactant dynamic models also include surfactant-based drug delivery systems. Consider the delivery pathway of a liquid medication drop as it makes its way from the trachea to the alveoli. It starts as a liquid plug, progresses to a deposited film lining the airways, establishes a surface layer, and finally reaches the alveolar compartment. The surface tension of a surfactant-coated layer depends on the local concentration of surfactant, which changes owing to flow, surface deformation, and surface diffusion of the molecule. Surface tension gradients caused by variations of surfactant concentration give rise to Marangoni flows that distribute the surfactant [16,17].

Flows of thin liquid films influenced by different types of surfactant constitute a complex area of research with various contributions by chemists, physicists, engineers, and mathematicians. The analysis of surface tension and surface-active agents in the dynamics of thin viscous liquid films is of interest in many applications in industrial coating, biomedical fields, or film drainage in emulsions and foams. Surfactants acting at the interface of a fluid film induce surface tension gradients that influence the dynamics of the fluid film. At the same time, the surfactant itself spreads along the interface due to the flow arising from those surface tension gradients. The latter aspect is called the Marangoni effect.

The lubrication approximation is the classical approach for studying the dynamics of thin viscous films. In spherical geometry, which is the one we adopt in our work, well-posedness of the thin film model was analyzed in [18,19]. The motion of a Newtonian viscous fluid layer on a solid horizontal plane with a monolayer of insoluble surfactant on its surface was modeled by Jensen and Grotberg [20] resulting in

$$\begin{cases} h_t + \frac{1}{3}(h^3(\mathcal{S}h_{xxx} - \mathcal{G}h_x + 3\mathcal{A}h^{-4}h_x))_x + \frac{1}{2}(h^2\sigma_x)_x = 0, & (1) \\ \Gamma_t + \frac{1}{2}(\Gamma h^2(\mathcal{S}h_{xxx} - \mathcal{G}h_x + 3\mathcal{A}h^{-4}h_x))_x + (\Gamma h\sigma_x)_x = (\mathcal{D}(\Gamma)\Gamma_x)_x, & (2) \end{cases}$$

where h is the film height, Γ is the surfactant concentration in the monolayer, $\sigma(\Gamma)$ is the surface tension which depends on surfactant concentration, $\mathcal{S}$ is a parameter related to the capillary forces (i.e., surface tension), $\mathcal{G}$ is the parameter characterizing the gravitational force directed vertically downward, $\mathcal{A}$ is related to the Hamaker constant and connected with intermolecular van der Waals forces, and $\mathcal{D}$ is related to the surface diffusivity of surfactants. This model is the generalization of the original system derived by Gaver and Grotberg [21] and studied in [22,23];

the new model includes a nonlinear equation of state and van der Waals forces. Capillarity is an important factor in stabilizing the film against instabilities due to van der Waals forces. The latter can cause a film to rupture. Since film rupture has such a dramatic effect on the spreading process, it interferes severely with methods of delivery of surfactant or drugs, making it of considerable importance to establish the conditions under which rupture might occur. Marangoni forces alone are not sufficient to induce the film thickness to reach zero in finite time, but they can deform the film to allow van der Waals forces to overcome the stabilizing effects of capillarity (and of the surfactant monolayer itself) and give rise to rupture and dry-out.

Various models are in use relating surface tension σ to surfactant concentration Γ. Under constant temperature, a fundamental equation of chemical thermodynamics relates the concentration dependent surface tension σ to the free energy, Φ, and the chemical potential, Φ', where both functions depend on the surfactant concentration Γ [24]:

$$\sigma(\Gamma) = \Phi(\Gamma) - \Gamma\Phi'(\Gamma). \tag{3}$$

By convexity of the free energy, this relation implies a monotonous decrease of surface tension for nonnegative concentration. It was confirmed by numerous experiments that the surface diffusivity of surfactant is not a constant [25–27], and can be modeled by a nonlinear function of the surfactant concentration Γ (see e.g., [28, (6.1) and (6.2), pp. 158–159]), namely,

$$\sigma(\Gamma) = (1+\theta\Gamma)^{-3}, \quad \mathcal{D}(\Gamma) = (1+\tau\Gamma)^{-k}, \tag{4}$$

where θ, τ, and k are some positive empirical parameters. In reality, the parameter θ depends on the material properties of the monolayer (cf. [28] for details). The empirical relation (4) is based on experimental data obtained for the inner subinterval $0 < \delta \le \sigma \le 1$. For example, if $\theta = 0.15$, then (4) well describes an oil layer on water [28, Fig. 2, p. 159] . It is very difficult to obtain high experimental accuracy when the surfactant concentration reaches near saturation levels.

In many applications, the dependence $\sigma(\Gamma)$ is taken to follow the Frumkin equation of state (cf. [29, (16), p. 324] for example):

$$\sigma(\Gamma) = \sigma_0 + 2.303RT\,\Gamma_s\big(b(\Gamma/\Gamma_s)^2 + \ln(1-\Gamma/\Gamma_s)\big), \tag{5}$$

where σ_0 is the surface tension of pure solvent and b is the Frumkin constant. Here, the restriction $\Gamma < \Gamma_s$ must hold. This equation, first formulated as an empirical relation, can be obtained from a general surface equation of state if one assumes ideal surface behavior (i.e., surface activity coefficients close to unity).

In this paper, we model and study the behavior of surfactant-driven thin film flow inside the alveoli shapes of which are considered to be approximately spherical, taking into account pulmonary surfactant production and recycling by Type 2 cells as well as its degradation. We model production of the surfactant by introducing a position-dependent source term, and we assume a uniform degradation rate for the surfactant. We also allow for the inflation and deflation of the alveolar compartment by taking the radius of the alveolus to be time periodic.

The article is structured as follows: in Sect. 2, we apply the lubrication approximation to derive and simplify the mathematical model; in Sect. 3, we carry out numerical simulations for the constant radius case; in Sect. 4, we present the numerical simulation results for the time-periodic case. Section 5 summarizes the results and discusses their significance.

2 Model formulation

In this section, we derive a mathematical model for the dynamics of the alveolar lining fluid on the inner surface of a spherical alveolus and the insoluble surfactant on its liquid–air interface. This derivation is analogous to our earlier work [30,31] which considered thin films on the outside of a sphere undergoing rotation or with thermal gradients.

With regard to the sphericity assumption, it should be noted that the alveoli of human lungs cluster together in alveolar sacs and these clusters are commonly said to resemble clusters of grapes, as the nearly spherical alveoli appear to bud away from the alveolar ducts. However, imaging studies show that alveoli are only approximately spherical and that describing the structure as "grape-like" would be an oversimplification. Polyhedral alveolar shapes have been observed [32] although in that case, the specimens had to be extensively prepared by instillation of glutaraldehyde in potassium phosphate buffer at a pressure of 20 cm H_2O [whereas total lung capacity (TLC) is usually determined at 30 cm H_2O in adult rats], which can affect alveolar shape and imaging. Nevertheless, future modeling studies should consider polyhedral shapes with the possibility that the fluid lining may accumulate at any corners. In this initial study, we begin with the assumption that the alveolus is a perfect sphere.

Consider a thin viscous liquid film on the inner surface of a sphere of time-dependent radius $R(t)$ in the presence of gravity and surface tension. We assume that the system is axisymmetric with respect to the gravitational axis. Let r denote the distance from origin at the center of the sphere, and θ the polar angle relative to the positive vertical axis. There is insoluble surfactant on the liquid–air interface, which is produced at rate $\alpha(\theta)$ which is related to the distribution of Type 2 alveoli cells and degrades with a constant rate constant β. The thickness of the thin liquid film is denoted by $h(\theta, t)$ and the concentration of surfactant is denoted by $\Gamma(\theta, t)$. The interface of the thin film $r = R(t) - h(\theta, t)$ is the zero-level set of function

$$\mathcal{F}(r, \theta, t) = r - R(t) + h(\theta, t).$$

The kinematic boundary condition $\mathrm{D}\mathcal{F}/\mathrm{D}t = 0$ reads

$$\frac{\partial h}{\partial t} = -v_r - \frac{v_\theta}{r}\frac{\partial h}{\partial \theta} + \dot{R}(t) \tag{6}$$

at the liquid–air interface $r = R(t) - h(\theta, t)$.

The continuity equation in spherical coordinates can be written as

$$\frac{1}{r^2}\frac{\partial}{\partial r}\left(r^2 v_r\right) + \frac{1}{r\sin\theta}\frac{\partial}{\partial \theta}(v_\theta \sin\theta) = 0.$$

Multiply this equation by $r^2 \sin\theta$ and integrate along r at a fixed θ to get

$$\sin\theta\,(r^2 v_r)\Big|_{R-h}^{R} + \frac{\partial}{\partial \theta}\int_{R-h}^{R} r v_\theta \sin\theta\,\mathrm{d}r - (r v_\theta \sin\theta)|_{R-h}\frac{\partial h}{\partial \theta} = 0. \tag{7}$$

Combining this with the kinematic boundary condition, along with the no-slip boundary condition $v_r = \dot{R}(t)$ at $r = R(t)$, we derive the time evolution equation

$$(R-h)^2\frac{\partial h}{\partial t} + \frac{\partial}{\partial \theta}\left(\int_{R-h}^{R} r v_\theta\,\mathrm{d}r\right) + \dot{R}(2Rh - h^2) = 0. \tag{8}$$

In order to get a self-contained partial differential equation for $h(\theta, t)$, we need to relate the velocity component v_θ to the film thickness.

We consider the standard lubrication form of the momentum equations from the Navier–Stokes equations (namely that the hydrostatically modified pressure is uniform across the film and the gradient of that pressure in the long direction balances the dominant viscous term), having the forms

$$\frac{\partial P}{\partial r} = 0, \tag{9}$$

$$\frac{1}{r}\frac{\partial P}{\partial \theta} = \frac{\mu}{r^2}\frac{\partial}{\partial r}\left(r^2\frac{\partial v_\theta}{\partial r}\right), \tag{10}$$

where P denotes the modified pressure field, which is defined by

$$P = p - \rho\,\mathbf{g}\cdot\mathbf{x} = p + \rho g\, r\cos\theta.$$

The normal stress balance at the liquid–air interface $r = R - h$ states that the pressure in the film needs to equal to the air pressure p_0 plus the capillary contribution given by $\sigma\nabla\cdot\mathbf{n}$, where σ is the surface tension dependent upon the surfactant concentration $\Gamma(\theta, t)$ and $\mathbf{n}$ is the normal unit vector pointing toward the air phase. Under the lubrication approximation, the normal stress balance simplifies to

$$P|_{r=R-h} = p_0 + \sigma\nabla\cdot\mathbf{n} = p_0 - \sigma\left(\frac{2}{R} + \frac{1}{R^2}\left(2h + \frac{1}{\sin\theta}\frac{\partial}{\partial\theta}\left(\sin\theta\frac{\partial h}{\partial\theta}\right)\right)\right). \tag{11}$$

From the r-momentum equation (9), we know that the modified pressure P is independent of r, and, thus, we have

$$P(\theta, t) = p_0 + \sigma\nabla\cdot\mathbf{n} + \rho g(R - h)\cos\theta.$$

By integrating the θ-momentum equation twice, the general solution for v_θ is found to be

$$v_\theta = \frac{1}{2\mu}\frac{\partial P}{\partial\theta}r - \frac{C_1}{r} + C_2. \tag{12}$$

The integration constants C_1 and C_2 can be obtained from the no-slip boundary condition at $r = R$ and the tangential stress balance at $r = R - h$:

$$\mathbf{n}\cdot(\boldsymbol{\tau}_2 - \boldsymbol{\tau}_1)\cdot\mathbf{t} = \nabla_s\sigma.$$

Here $\boldsymbol{\tau}_1$ and $\boldsymbol{\tau}_2$ are the viscous stresses in the liquid and air phases, respectively, the latter being negligible compared to the former. In our model, due to the presence of surfactant, surface tension σ is a function of surfactant concentration $\Gamma(\theta, t)$; thus σ is also a function of θ and t. Expanding the tangential stress balance along the θ direction and simplifying under the lubrication approximation yield

$$\mu r\frac{\partial}{\partial r}\left(\frac{v_\theta}{r}\right) = \frac{1}{r}\frac{\partial\sigma}{\partial\theta}, \tag{13}$$

at the interface $r = R - h$. Applying this boundary condition and the no-slip condition at $r = R$ enables the integration constants to be obtained as

$$C_1 = -\frac{R^2(R-h)}{2\mu(R+h)}\frac{\partial P}{\partial\theta} + \frac{R(R-h)}{\mu(R+h)}\frac{\partial\sigma}{\partial\theta}, \qquad C_2 = -\frac{R^2}{\mu(R+h)}\frac{\partial P}{\partial\theta} + \frac{(R-h)}{\mu(R+h)}\frac{\partial\sigma}{\partial\theta}.$$

Upon inserting these into the expression for v_θ and evaluating its integral as it appears in the evolution equation (8) and making use of the assumption that $h \ll R$, we obtain the leading-order governing equation for $h(\theta, t)$:

$$\frac{\partial h}{\partial t} - \frac{1}{R^2\sin\theta}\frac{\partial}{\partial\theta}\left(\frac{h^3\sin\theta}{3\mu}\frac{\partial P}{\partial\theta} - \frac{h^2\sin\theta}{2\mu}\frac{\partial\sigma}{\partial\theta}\right) + \frac{2h}{R}\dot{R}(t) = 0, \tag{14}$$

where

$$P(\theta, t) = \rho g R \cos\theta - \frac{\sigma}{R^2}\left(2h + \frac{1}{\sin\theta}\frac{\partial}{\partial\theta}\left(\sin\theta\frac{\partial h}{\partial\theta}\right)\right). \tag{15}$$

The total mass or volume of the alveolar fluid is conserved, i.e.,

$$\frac{\mathrm{d}}{\mathrm{d}t}\int_{R-h}^{R}\int_{0}^{\pi} h(\theta, t) r^2 \sin\theta \,\mathrm{d}r \,\mathrm{d}\theta = 0, \tag{16}$$

which can be simplified after applying the lubrication approximation to the form:

$$\frac{\mathrm{d}}{\mathrm{d}t}\left(R^2(t)\int_{0}^{\pi} h(\theta, t)\sin\theta \,\mathrm{d}\theta\right) = 0. \tag{17}$$

Surface tension σ depends on the surfactant concentration, $\sigma = \sigma(\Gamma)$, and Γ satisfies the interface transport equation (e.g., see [33])

$$\frac{\mathrm{D}\Gamma}{\mathrm{D}t} + (\nabla_\mathrm{s}\cdot\mathbf{v_s})\Gamma + (\nabla_\mathrm{s}\cdot\mathbf{n})v_n\Gamma = \nabla_\mathrm{s}\cdot(D_\mathrm{s}\nabla_\mathrm{s}\Gamma) + \alpha - \beta\Gamma, \tag{18}$$

where α describes the production of surfactant, β is the degradation rate, $\mathrm{D}/\mathrm{D}t = \partial/\partial t + \mathbf{v_s}\cdot\nabla_\mathrm{s}$, $v_n = \mathbf{v}\cdot\mathbf{n}$ and ∇_s is the surface gradient which can be defined as $(\mathbf{I} - \mathbf{nn})\cdot\nabla$. Since our model is one of an insoluble surfactant, by necessity the production and degradation rates of surfactant are also confined to the interface. However, an interpretation of the production rate α, which is taken to be spatially varying, is that it is the largest in the vicinity of the underlying Type 2 cells that are the true sources of surfactants. The transport process involving diffusion of surfactant from the Type 2 cells through the fluid layer and its adsorption/desorption upon the interface itself can be built into more sophisticated future modeling efforts involving soluble surfactant.

Under the lubrication assumptions, we can approximate $\mathbf{v_s} \approx v_\theta\mathbf{e}_\theta$, $v_n \approx -\dot{R}$ and $\mathbf{n} \approx -\mathbf{e_r}$. Thus, we can simplify Eq. (18) as

$$\frac{\partial\Gamma}{\partial t} + \frac{1}{R\sin\theta}\frac{\partial}{\partial\theta}(v_\theta\Gamma\sin\theta) + \frac{2\dot{R}}{R}\Gamma = \frac{1}{R^2\sin\theta}\frac{\partial}{\partial\theta}\left(\sin\theta D_\mathrm{s}\frac{\partial\Gamma}{\partial\theta}\right) + \alpha(\theta) - \beta\Gamma. \tag{19}$$

Substituting the expression for v_θ at $r = R - h$, and using the lubrication approximation $h \ll R$, we obtain

$$\frac{\partial\Gamma}{\partial t} + \frac{1}{\sin\theta}\frac{\partial}{\partial\theta}\left(\frac{\sin\theta}{\mu R^2}\left(\frac{\partial\sigma}{\partial\theta}h - \frac{1}{2}\frac{\partial P}{\partial\theta}h^2\right)\Gamma\right) = \frac{1}{\sin\theta}\frac{\partial}{\partial\theta}\left(\frac{D_\mathrm{s}}{R^2}\sin\theta\frac{\partial\Gamma}{\partial\theta}\right) + \alpha(\theta) - \left(\beta + \frac{2\dot{R}}{R}\right)\Gamma. \tag{20}$$

In the absence of production and degradation of the surfactant, i.e., when $\alpha = \beta = 0$, the total amount of surfactant satisfies the total mass conservation

$$\frac{\mathrm{d}}{\mathrm{d}t}\left(R^2(t)\int_{0}^{\pi}\Gamma(\theta, t)\sin\theta \,\mathrm{d}\theta\right) = 0. \tag{21}$$

When the production and degradation of surfactant are present, the total amount of surfactant at steady state, Γ_0, satisfies

$$\int_{0}^{\pi}\alpha(\theta)\sin\theta \,\mathrm{d}\theta = \beta\Gamma_0. \tag{22}$$

After the change of variable $x = -\cos\theta$, the coupled system of evolution equations for $h(\theta, t)$ (14) and $\Gamma(\theta, t)$ (20) and their conservation properties (17) and (22) can be written more compactly as

$$\frac{\partial h}{\partial t} + \frac{\partial}{\partial x}\left(h^2(1-x^2)\left[Q_1 h + \frac{1}{2}Q_2\right]\right) + 2h\frac{\dot{R}(t)}{R(t)} = 0, \tag{23}$$

$$\frac{\partial \Gamma}{\partial t} + \frac{\partial}{\partial x}\left(h\Gamma(1-x^2)\left[\frac{3}{2}Q_1 h + Q_2\right]\right) = \frac{\partial}{\partial x}\left(\frac{D_s}{R^2(t)}(1-x^2)\frac{\partial \Gamma}{\partial x}\right) + \alpha - \left(\beta + \frac{2\dot{R}}{R}\right)\Gamma, \tag{24}$$

and

$$\frac{\mathrm{d}}{\mathrm{d}t}\left(R^2(t)\int_{-1}^{1} h\,\mathrm{d}x\right) = 0, \tag{25}$$

$$\int_{-1}^{1} \alpha\,\mathrm{d}x = \beta\Gamma_0, \tag{26}$$

where

$$Q_1(h, \Gamma, x, t) = \frac{\rho g}{3\mu R(t)} + \frac{\sigma(\Gamma)}{3\mu R^4(t)}\frac{\partial}{\partial x}\left(2h + \frac{\partial}{\partial x}\left((1-x^2)\frac{\partial h}{\partial x}\right)\right), \tag{27}$$

and

$$Q_2(\Gamma, x, t) = \frac{1}{\mu R^2(t)}\frac{\partial \sigma(\Gamma)}{\partial x}. \tag{28}$$

2.1 Assumed forms of $\sigma(\Gamma)$ and $R(t)$

Equations (23) and (24) provide a coupled system of equations involving $h(x, t)$ and $\Gamma(x, t)$. To close the system, one more relation that we need to specify is the dependence of σ upon Γ. While a number of such relations have been stipulated and used previously, as mentioned in the Sect.1, here we adopt a novel relation based on the observation that over a wide range of alveolar volumes, the pressure differential needed to inflate the lungs remains relatively constant. In order for the pressure jump across the alveolar fluid interface to remain nearly constant as the radius of the alveolus changes, surface tension must also change in order to keep the Laplace pressure constant. Consider an idealized state in the absence of gravity where the thin film coating the inside of the sphere modeling the alveolus is uniform and the surfactant distribution is also uniform. Assume that the Laplace pressure difference $\Delta p = 2\sigma/R$ is constant with respect to R and see for what dependence $\sigma = \sigma(\Gamma(R))$ this would be possible. Since the surfactant is insoluble and the total amount of surfactant is conserved, we have $\Gamma \propto 1/R^2$. Thus, only when $\sigma(\Gamma) = c_0/\sqrt{\Gamma}$ where c_0 is a constant would the Laplace pressure remain constant. To obtain the constant c_0, we appeal to experimental measurements that show that when Γ is at its minimum, corresponding to the maximum alveolar radius, $\sigma(\Gamma)$ assumes its maximum value of approximately $\sigma_0 = 25$ mN/m. We recognize that this is a drastic assumption and ignore the role of parenchymal elasticity, which certainly plays a role when surface tension effects have been reduced due to the presence of surfactant. Nevertheless, as a model that makes the Laplace pressure relatively independent of lung volume, it would seem to be a reasonable starting point for modeling.

To model the time dependence of the radius of the alveoli, we appeal to the physiological parameter: percentage of TLC. Let us assume that the radius of an alveolus is a periodic function of time with the form

$$R(t) = R_0(1 - R_m + R_m\cos(\omega t)),$$

where $R_0 > 0$ the maximum radius, and R_m the dimensionless oscillation amplitude, restricted to the range $0 < R_m < 0.5$. The alveolus has a radius of R_0 at peak inflation and one of $R_0(1 - 2R_m)$ at maximum exhalation. TLC is defined as the volume in the lungs at maximum inflation, so the fraction of TLC at time t (if all alveoli inflate

and deflate in unison) is given by $(R(t)/R_0)^3$. Physiologically, the percentage of TLC varies from 20 to 100% during spontaneous breathing; the approximation $R_m \approx 0.2$ puts us near the lower end of that range. It should be noted that another possible model for changes in lung volume for which experimental evidence has been gathered is based not on inflation in unison of all the alveoli, but on the so-called recruitment/derecruitment of alveoli that, more or less, maintain their individual volumes [34]. Even in that case, however, when new alveoli are initially recruited as lung volume starts to increase, there must be some initial inflation of the new alveoli to their nearly constant volume.

2.2 Scaling and non-dimensionalization

In this subsection, we rewrite the evolution equations in scaled form and obtain the dimensionless groups that represent gravity, surface tension, and Marangoni effects. Let H be the average thickness of the thin film when the spherical alveolus reaches its maximum radius R_0. The equations we have derived are valid to leading order in the lubrication parameter $\epsilon = H/R_0$ with corrections (not included here) being $\mathcal{O}(\epsilon)$. We list the physical parameters at that state in Table 1, some of which are taken from reference [35]. We define dimensionless parameters $\hat{h} = h/H$ and $\hat{\Gamma} = \Gamma/\Gamma_0$ and define τ as an arbitrary time scale for the time being. The dimensionless equations take the forms

$$\frac{\partial \hat{h}}{\partial \hat{t}} + \frac{\partial}{\partial x}\left(\hat{h}^2(1-x^2)\left[\hat{Q}_1\hat{h} + \frac{1}{2}\hat{Q}_2\right]\right) + 2\hat{h}\frac{\dot{\hat{R}}}{\hat{R}} = 0, \tag{29}$$

$$\frac{\partial \hat{\Gamma}}{\partial \hat{t}} + \frac{\partial}{\partial x}\left(\hat{h}\hat{\Gamma}(1-x^2)\left[\frac{3}{2}\hat{Q}_1\hat{h} + \hat{Q}_2\right]\right) = \frac{\partial}{\partial x}\left(\frac{\mathcal{D}}{\hat{R}^2}(1-x^2)\frac{\partial \hat{\Gamma}}{\partial x}\right) + \frac{\alpha\tau}{\Gamma_0} - \left(\beta\tau + \frac{2\dot{\hat{R}}}{\hat{R}}\right)\hat{\Gamma}, \tag{30}$$

where

$$\hat{Q}_1(\hat{h}, \hat{\Gamma}, x, \hat{t}) = \frac{\mathcal{G}}{\hat{R}} + \frac{\mathcal{S}\hat{\sigma}(\hat{\Gamma})}{\hat{R}^4}\frac{\partial}{\partial x}\left(2h + \frac{\partial}{\partial x}\left((1-x^2)\frac{\partial \hat{h}}{\partial x}\right)\right), \tag{31}$$

Table 1 Values of the physical parameters when $R(t) = R_0$, the dimensionless groups, and some of their ratios

Parameters	Units	Values
σ_0	N/m	2.5×10^{-2}
g	m/s^2	9.8
ω	1/s	$\pi/2$
ρ	kg/m^3	10^3
μ	Pa s	10^{-3}
R_0	m	10^{-4}
H	m	10^{-6}
D_s	m^2/s	10^{-9}
β	1/s	5.6×10^{-5}
$\epsilon = H/R_0$	1	10^{-2}
$\mathcal{G} = \tau\rho g H^2/(3\mu R_0)$	1	$3.3 \times 10^{-2}\tau$
$\mathcal{S} = \tau\sigma_0 H^3/(3\mu R_0^4)$	1	$8.3 \times 10^{-2}\tau$
$\mathcal{M} = \tau\sigma_0 H/(\mu R_0^2)$	1	$2.5 \times 10^3\tau$
$\mathcal{D} = \tau D_s/R_0^2$	1	0.1τ
$\mathcal{G}/\mathcal{S}$	1	0.4
$\mathcal{S}/\mathcal{M}$	1	3.3×10^{-5}

and

$$\hat{Q}_2(\hat{\Gamma}, x, \hat{t}) = \frac{\mathcal{M}}{\hat{R}^2}\frac{\partial \hat{\sigma}(\hat{\Gamma})}{\partial x} \tag{32}$$

with

$$\hat{R}(\hat{t}) = \frac{R}{R_0} = 1 - R_\mathrm{m} + R_\mathrm{m}\cos(\omega\tau\hat{t}), \quad \hat{\sigma}(\hat{\Gamma}) = \frac{\sigma(\hat{\Gamma})}{\sigma_0} = (2\hat{\Gamma})^{-1/2}. \tag{33}$$

The dimensionless relation between $\hat{\sigma}$ and $\hat{\Gamma}$ is based on the assumption outlined in Sect. 2.1 such that $\hat{\sigma}$ attains its maximum value of 1 when a uniformly distributed $\hat{\Gamma}$ reaches its minimum value of 0.5. Four dimensionless groups appear in these equations, defined by

$$\mathcal{G} = \frac{\tau\rho g H^2}{3\mu R_0}, \quad \mathcal{S} = \frac{\tau\sigma_0 H^3}{3\mu R_0^4}, \quad \mathcal{M} = \frac{\tau\sigma_0 H}{\mu R_0^2}, \quad \mathcal{D} = \frac{\tau D_\mathrm{s}}{R_0^2}. \tag{34}$$

These equations characterize gravity, surface tension, Marangoni effect, and surface diffusion, respectively. In addition, the combination $\omega\tau$ represents the dimensionless frequency of the time-periodic breathing.

In Table 1, we collect the approximate experimental values of the parameters that relate to this system. We take the average radius of the alveoli to be approximately 0.1 mm or 100 μm. The value of β comes from assuming the half-life for the degradation of the surfactant to be about 5 h (while, in actuality, it may be as long as 24 h). We calculate the dimensionless groups using experimental values. We find that the gravity parameter $\mathcal{G}$, the surface tension parameter $\mathcal{S}$, and the diffusion parameter $\mathcal{D}$ are comparable, while the Marangoni number $\mathcal{M}$ is much larger than the other three groups. As we will see in the simulations, this causes the Marangoni effects to take place on a faster time scale, while the other effects determine the longer time dynamics.

For the rest of this paper, we will do simulations based on the Eqs. (29)–(34). We will drop the hats from the variables in the equation for notational convenience. We choose the time scale τ such that $\mathcal{S} = 1$, which implies that $\tau \approx 12$ s, leading to $\mathcal{G} \approx 2.5$, $\mathcal{M} \approx 3 \times 10^4$ and $\mathcal{D} \approx 1.2$. We also point out that $\beta\tau = 6.72 \times 10^{-4} \ll 1$, consistent with having a relatively long degradation time compared to the time scale for gravitational drainage of the film or that for surface tension to act, and $\omega\tau = 18.8$, which implies that the period of oscillations $(2\pi/\omega)$ is about three times smaller than the time scale $\tau = 12$ s.

3 The constant-radius case

In this section, in order to understand the roles of surface tension, gravity, and Marangoni effects without the complicating factor of changing radius, we study the model under the assumption that the radius of the alveolus is constant. All simulations are carried out using COMSOL Multiphysics. The next section considers the non-constant radius case where it is shown that through certain changes of variables, the equations can be simplified and analyzed without further detailed numerical simulations. Under the condition that $R(t) \equiv 1$, the simplified equations are

$$\frac{\partial h}{\partial t} + \frac{\partial}{\partial x}\left[h^3(1-x^2)\left(\mathcal{G} + \frac{\mathcal{S}}{\sqrt{2\Gamma}}\frac{\partial}{\partial x}\left(2h + \frac{\partial}{\partial x}\left((1-x^2)\frac{\partial h}{\partial x}\right)\right)\right) - \frac{\mathcal{M}(1-x^2)}{2(2\Gamma)^{3/2}}\frac{\partial \Gamma}{\partial x}h^2\right] = 0, \tag{35}$$

$$\frac{\partial \Gamma}{\partial t} + \frac{\partial}{\partial x}\left[\frac{3}{2}h^2\Gamma(1-x^2)\left(\mathcal{G} + \frac{\mathcal{S}}{\sqrt{2\Gamma}}\frac{\partial}{\partial x}\left(2h + \frac{\partial}{\partial x}\left((1-x^2)\frac{\partial h}{\partial x}\right)\right)\right) - \frac{\mathcal{M}(1-x^2)}{(2\Gamma)^{3/2}}\frac{\partial \Gamma}{\partial x}h\Gamma\right]$$
$$= \frac{\partial}{\partial x}\left(\mathcal{D}(1-x^2)\frac{\partial \Gamma}{\partial x}\right) + \frac{\alpha\tau}{\Gamma_0} - \beta\tau\Gamma. \tag{36}$$

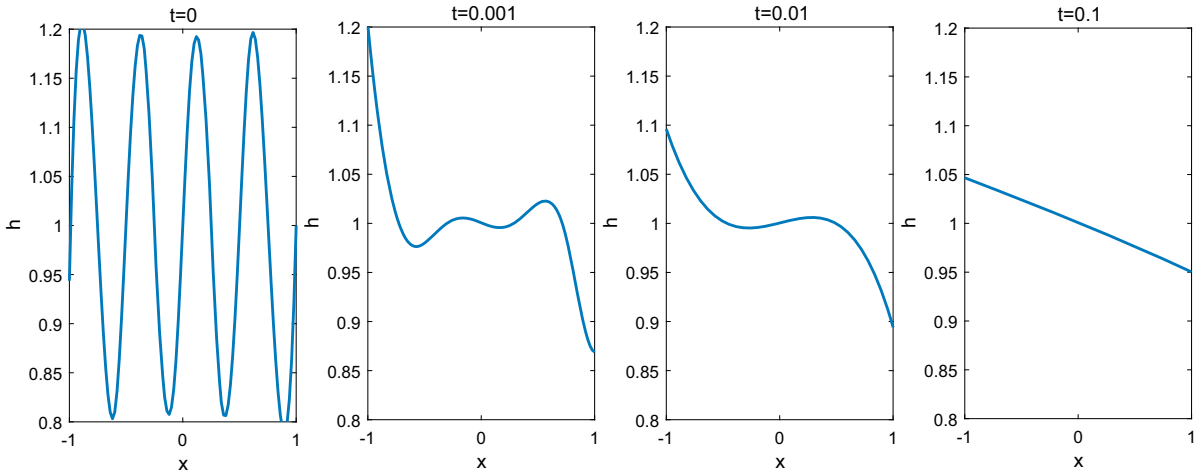

Fig. 2 $h(x, t)$ at times $t = 0, 0.001, 0.01$, and 0.1 with initially a constant surfactant distribution. Surface tension and Marangoni effect are considered in the absence of gravity

To start with, we only consider the surface tension and Marangoni effects. For the simulations, we thus take $\mathcal{G} = \alpha = \beta = 0$ and $\mathcal{S} = 1$, $\mathcal{M} = 3 \times 10^4$ and $\mathcal{D} = 1.2$. Figure 2 shows the evolution of the film thickness starting with a sinusoidal perturbation but with an initially uniform surfactant distribution $\Gamma \equiv 0.5$. Surface tension drives the perturbed initial profile toward a state with uniform curvature and minimal area (i.e., an overall spherical shape) and the surfactant distribution will return to its constant state (not shown). We can observe from Fig. 2 that the final steady state of $h(x)$ is not a constant but a linear function of x. This is because in the absence of gravity, the final equilibrium state of the film, while having an overall spherical interface, need not have its center at the geometric center of the alveolus: the spherical alveolar fluid interface can be shifted slightly up or down (corresponding the film profile $h(\theta) = 1 + \varepsilon \cos\theta$ with a small ϵ) and cause the steady-state solution $h(x)$ not to be constant but to vary linearly in $x = -\cos\theta$. Depending on the initial perturbation in h, the inner spherical interface may end up shifted up or down relative to the outer spherical boundary of the alveolus.

With a nonuniform initial Γ distribution, surface tension and surface diffusion will still stabilize the system and drive h and Γ to uniform states as time tends to infinity, but the transient evolution is more complex. Figures 3 and 4 show the short- and long-time dynamics of the system, respectively, starting with an initial surfactant distribution that is highly concentrated near the equator of the spherical alveolus ($\theta = \pi/2$ or $x = 0$). As seen in Fig. 3, the film thickness will exhibit some initial waviness for very short times: the high concentration of surfactant at the equator will cause the film to get thinner there very quickly as the Marangoni effect drives the film away from that low-tension area; meanwhile, due to Marangoni effects, the distribution of surfactant becomes nearly uniform very quickly during this same time. Over a longer time, as seen in Fig. 4, surface tension will drive h toward a uniform distributions, while surface diffusion maintains the surfactant distribution near its uniform equilibrium state. To see the mathematical basis for the very rapid initial redistribution of surfactant, we can expand the x-derivative acting on the $\mathcal{M}$ term in Eq. (36) and combine it with the expanded term in the right-hand side. The coefficient of the diffusion term $\partial^2\Gamma/\partial x^2$ becomes $\mathcal{M}(2\Gamma)^{-3/2}(1 - x^2)h\Gamma + \mathcal{D}(1 - x^2)$, in which the $\mathcal{M}$ term dominates the $\mathcal{D}$ term, having a magnitude of order of 10^4. As such, the Marangoni term behaves as a diffusion effect and causes Γ to become nearly constant on a diffusion time scale of 10^{-4}. The relatively large Marangoni term thus causes any surfactant deposited on the alveolar fluid (e.g., by means of aerosolized drops) to quickly spread and cover the entire interface; while this can cause initial non-uniformities in the thickness of the alveolar fluid film, over a longer time, surface tension drives that back toward a uniform state.

Although intuition might suggest that gravitational effects are negligible on the very small length scales of the alveolus and the thin film, the above scaling which leads to a parameter $\mathcal{G}$ of order unity, comparable to the surface tension effect $\mathcal{S}$, suggests that gravity does play some role even at the alveolus scale. If we take gravity into con-

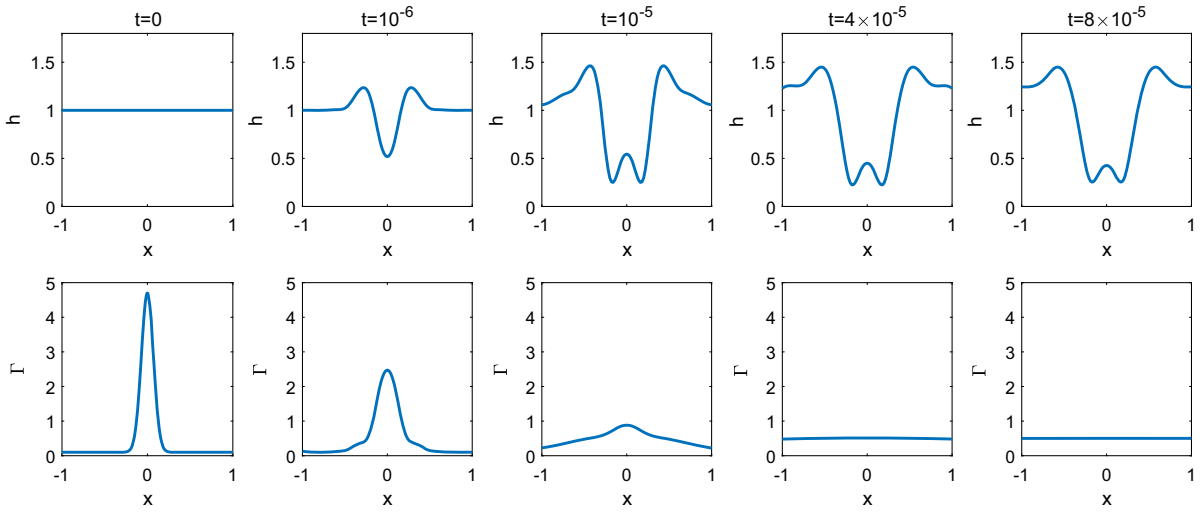

Fig. 3 $h(x,t)$ (top) and $\Gamma(x,t)$ (bottom) at times $t = 0, 10^{-6}, 10^{-5}, 4 \times 10^{-5}$, and 8×10^{-5} with a non-uniform initial surfactant distribution concentrated around the equator of the sphere. Surface tension and Marangoni effect are considered with no gravity. The short-time dynamics are seen in these plots

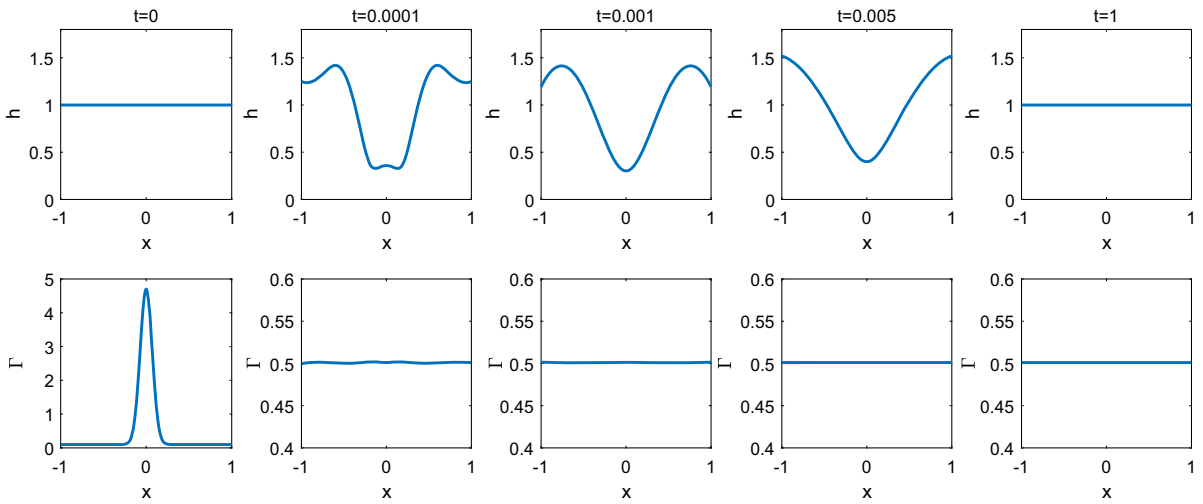

Fig. 4 $h(x,t)$ (top) and $\Gamma(x,t)$ (bottom) at times $t = 0, 0.0001, 0.001, 0.005$, and 0.1 with a non-uniform initial surfactant distribution concentrated at the equator. Surface tension and Marangoni effect are included but with no gravity. The longer-time dynamics are evident in these plot

sideration, Fig. 5 shows that it will drive the thin film toward the bottom of the alveolus. As seen in the top row of that figure, after a dimensionless time of 10, the thickness profile is about three times larger than its starting value at the south pole (i.e., at $\theta = \pi$ or $x = 1$). Interestingly, the profile is not monotonic and achieves its minimum not at the north pole, but slightly away from that. Since the Marangoni coefficient $\mathcal{M}$ is still large compared to the other coefficients, $\Gamma(x,t)$ remains nearly constant as seen in the bottom row of the figure (the vertical scale expands the immediate neighborhood of $\Gamma = 0.5$).

In order to see what happens if the Marangoni parameter is not quite that large or when it is turned off completely, we compare the cases with a much smaller Marangoni parameter and with no Marangoni effect in Fig. 6. The top and bottom rows in the figure show the evolutions of the film profile when $\mathcal{M}$ are 3 and 0, respectively. These appear fairly similar except that the film thicknesses at the south pole in the first row are slightly thinner than those in the

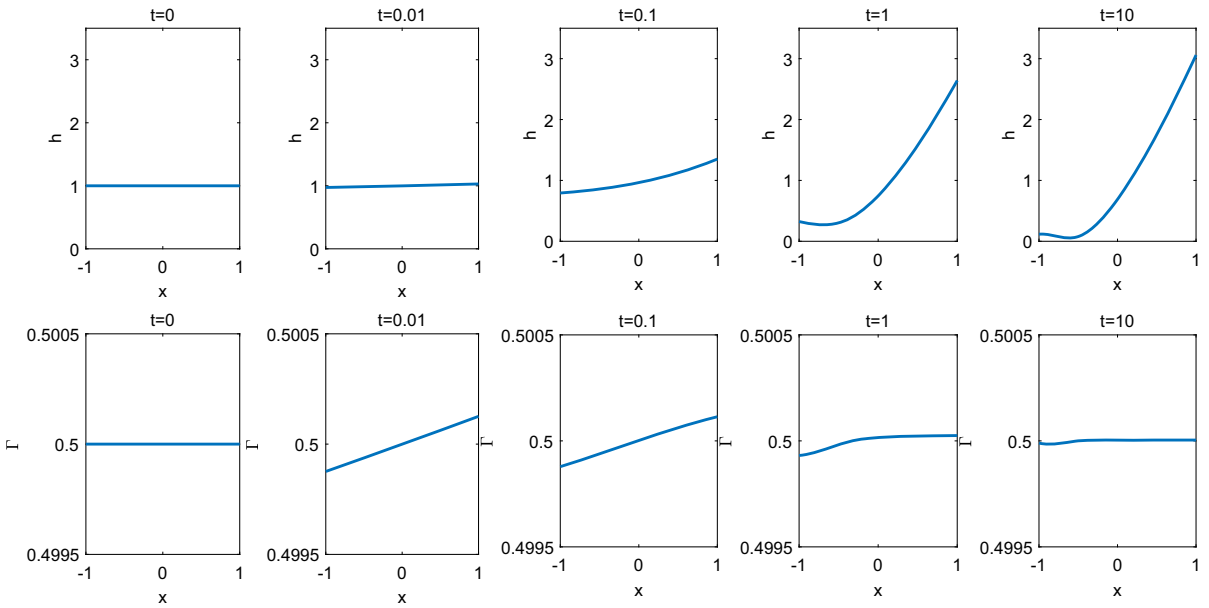

Fig. 5 $h(x,t)$ (top) and $\Gamma(x,t)$ (bottom) at times $t = 0, 0.01, 0.1, 1$, and 10 with an initially uniform surfactant distribution. Gravity, surface tension, and Marangoni effects are included. The film becomes the thickest near the bottom due to gravitational drainage, while surfactant concentration stays relatively constant

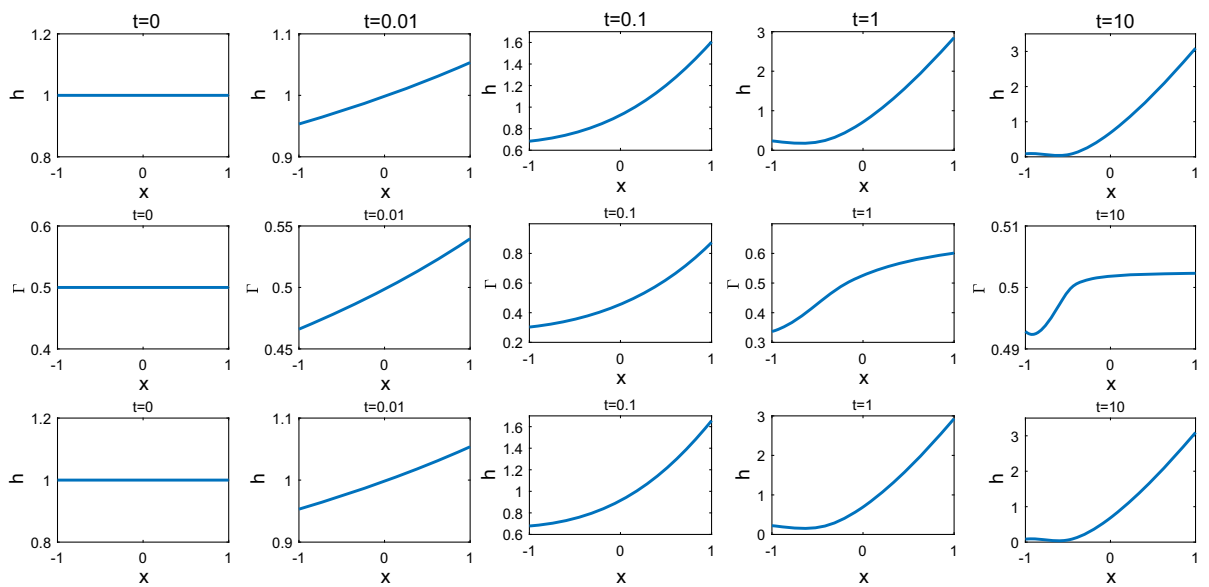

Fig. 6 $h(x,t)$ (top) and $\Gamma(x,t)$ (middle) for $\mathcal{M} = 3$, and $h(x,t)$ (bottom) without any surfactant, at times $t = 0, 0.01, 0.1, 1$, and 10 with an initially uniform surfactant distribution. Gravity, surface tension, and Marangoni effects are included. The evolution of the film is not affected much by the presence of surfactants; the film drains toward the bottom, and causes a transient redistribution of surfactants when present. To continue the computations beyond $t = 10$ when the film becomes extremely thin near (but not at) the north pole, one should include intermolecular forces in the model, although these may lead to finite-time rupture of the film

third row (the film thicknesses at south pole in the first row are 1, 1.053, 1.606, 2.85, and 3.092 and the thicknesses at the south pole in the third row are 1, 1.054, 1.656, 2.931, and 3.093). This shows that adding surfactant to the system with a Marangoni number of order unity will slow down the drainage due to gravity only slightly, despite the

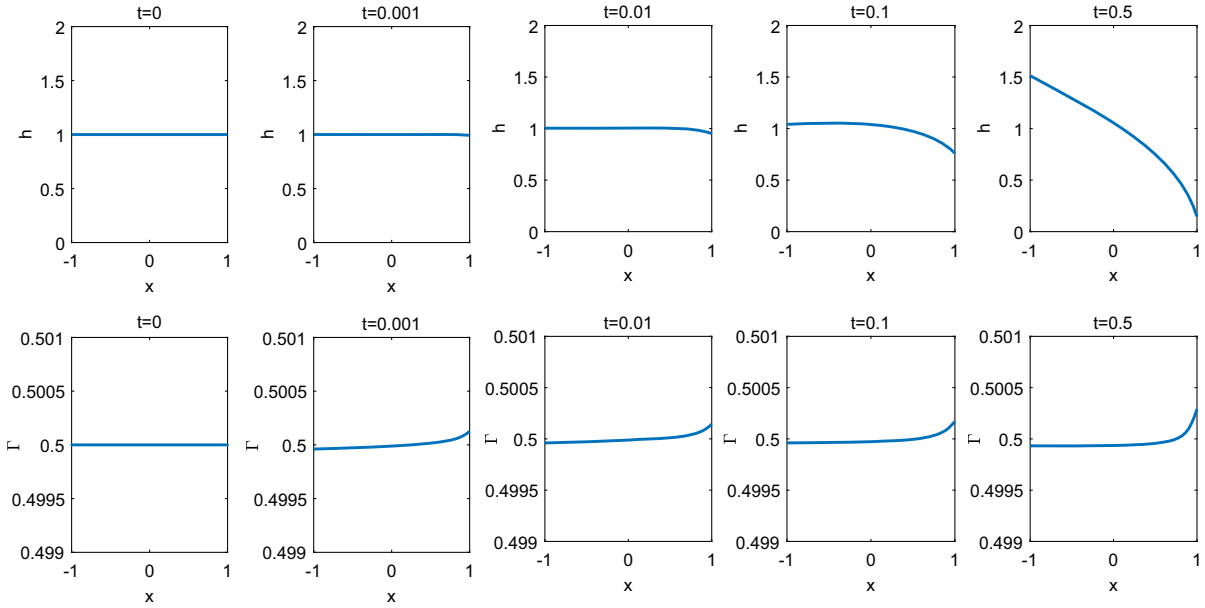

Fig. 7 $h(x,t)$ (top) and $\Gamma(x,t)$ (bottom) at times $t = 0, 0.001, 0.01, 0.1$, and 0.5 with a source concentrated at the bottom: $x = 1$. Surface tension and Marangoni effects are included, but gravity is absent. The presence of the source causes the film to become thinnest at the source and thickest at the opposite pole. Surfactant concentration is slightly higher near the source but fairly uniform away from that

visible redistribution of surfactants. The middle row shows the evolution of surfactant concentration Γ for $\mathcal{M} = 3$. In this case, surfactant concentration can deviate more from its equilibrium value of 0.5 and take longer to return to a uniform state compared to the earlier results at the much higher value of the Marangoni parameter.

At this point, we also add the surfactant production and degradation terms into the analysis. In order to observe the effects caused by these more clearly, we perform the simulations in the absence of gravity. After scaling, in order to make the total amount of surfactant constant, we need $\int_{-1}^{1}(\alpha/\Gamma_0)\,\mathrm{d}x = \beta$. We consider a strong source of surfactant that is concentrated at the bottom of the sphere. In this case, extra surfactant concentration will cause lower surface tension at the bottom and lead to an upward flow along the walls of the alveolus. We do the simulation using $\beta = 1$ and $\alpha(x)/\Gamma_0 = 11.284 \times \exp[-100(x-1)^2]$, and the result is shown in Fig. 7. In the top row, we observe that the film initially thins out at the south pole (near $x = 1$) and gradually assumes a monotonic profile which is the thickest at the north pole away from the source and thinnest at the bottom where the source is located. The surfactant concentration, observed in the bottom rows, shows a slight maximum near the source but is relatively uniform away from it. This suggests that if Type 2 cells in the alveoli are the sources of pulmonary surfactant, the alveolar fluid layer may be thinnest just above those Type 2 cells.

Appendix A considers the limiting case without Marangoni effects but with surface tension and weak gravity. It is seen that the presence of gravity, however small, precludes the existence of steady solutions without touchdown points or dry zones on the surface.

4 Non-constant radius case

In this section, we consider the case where the radius of the spherical alveolus changes with respect to time periodically. We take the scaled radius to be given by Eq. (33), with the full evolution equations given in Eqs. (29)–(33). We run the simulations using the experimental parameters from Table 1, except that we choose a moderate Marangoni number $\mathcal{M} = 3$ in order not to overwhelm the other effects by the fast-acting Marangoni term.

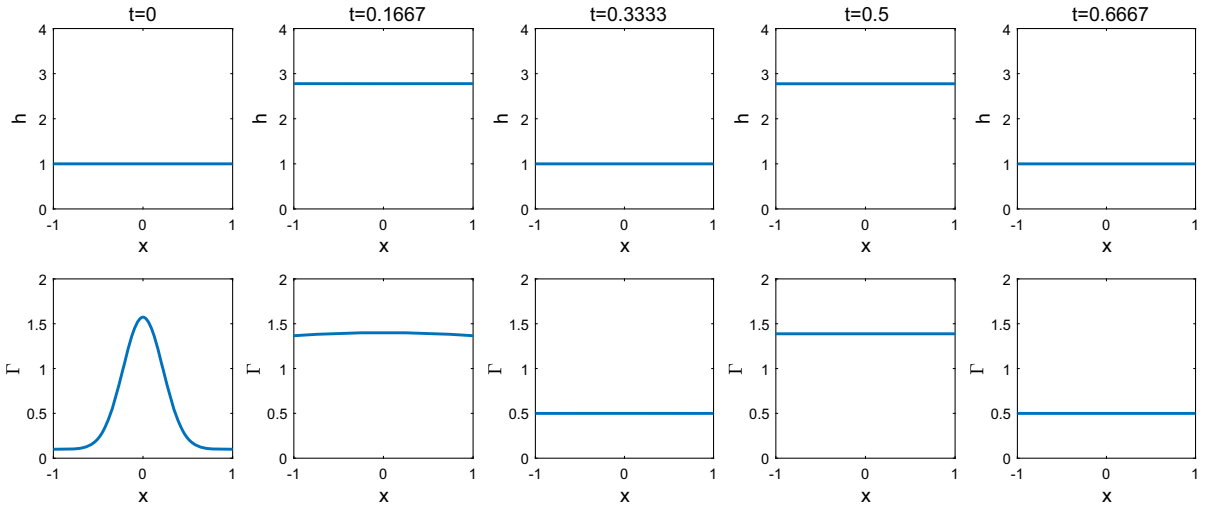

Fig. 8 $h(x,t)$ (top) and $\Gamma(x,t)$ (bottom) at times $t = 0, 0.1667, 0.3333, 0.5$, and 0.6667. The sphere radius changes periodically with time. Surface tension and Marangoni effects are included, but gravity is absent. The first, third, and fifth columns are when the sphere is at its maximum radius, and the second and fourth columns are when the sphere is with its minimum radius

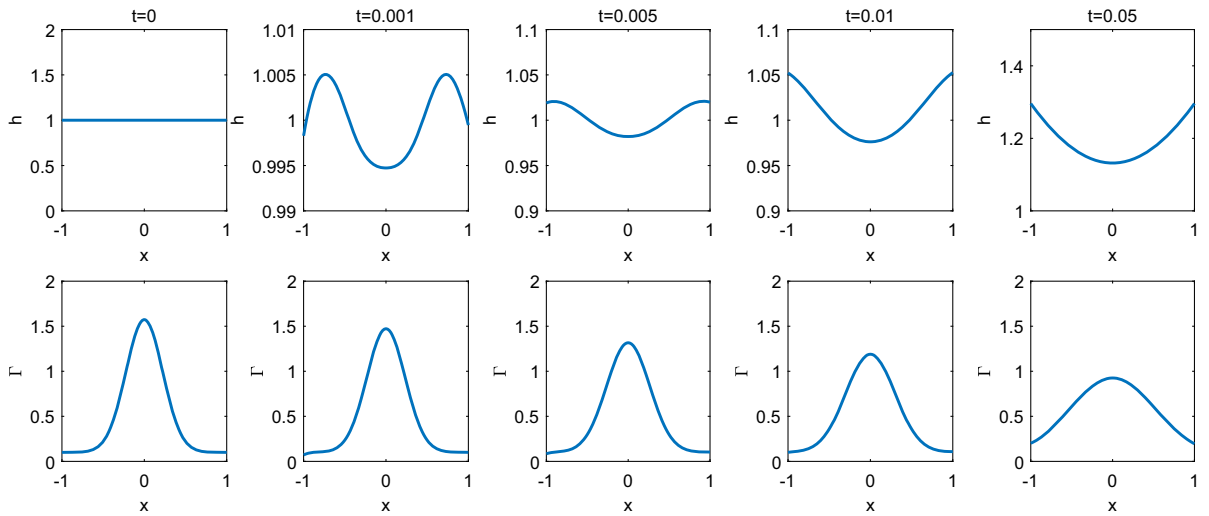

Fig. 9 $h(x,t)$ (top) and $\Gamma(x,t)$ (bottom) at times $t = 0, 0.001, 0.005, 0.01$, and 0.05. The sphere radius changes periodically with time. Surface tension and Marangoni effects are included, but gravity is absent

We first study the case in the absence of gravity. Long-time and short-time behaviors are shown in Figs. 8 and 9, respectively. The period of oscillations is $1/3$, and the time difference between adjacent columns in Fig. 8 is half of a period. We see from the figure that both h and Γ are nearly uniform at later times, but their values change due to the change of radius, in order to conserve mass. The first, third, and fifth columns correspond to times when the radius of the alveolus is at its maximum, at which times, the values of h and Γ reach their minimum, while the second and fourth columns are the opposite. For short times, Fig. 9 shows the result within half of a period. We see that the results are similar to Fig. 3, but the average values of h and Γ are increasing due to the initial decrease in the radius of the alveolus.

In the presence of gravity, long-time and short-time simulations are shown in Figs. 10 and 11, respectively. A dry zone appears near the top due to gravity when time gets large. Figure 10 also shows that the monotonicity of Γ changes when the radius of the sphere reaches its maximum and minimum values.

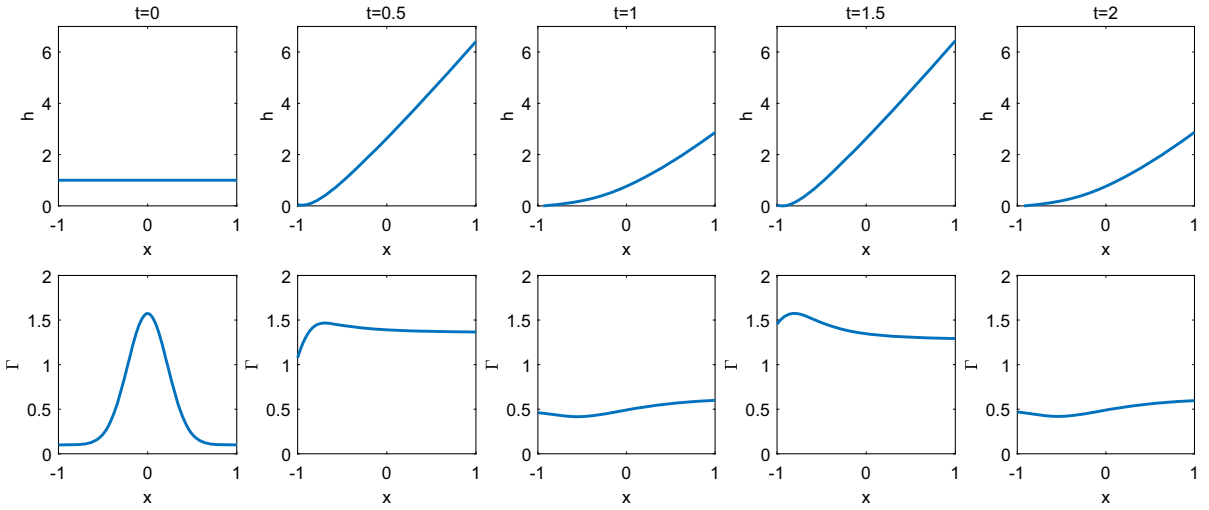

Fig. 10 $h(x,t)$ (top) and $\Gamma(x,t)$ (bottom) at times $t = 0$, 0.5, 1, 1.5, and 2. The sphere radius changes periodically with time. Gravity, surface tension, and Marangoni effects are included

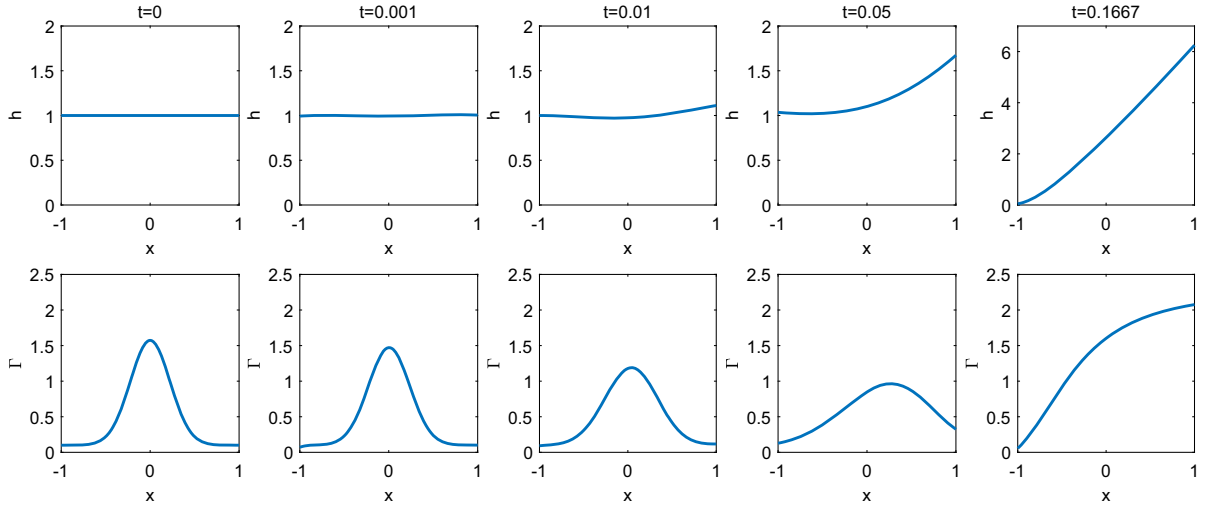

Fig. 11 $h(x,t)$ (top) and $\Gamma(x,t)$ (bottom) at times $t = 0$, 0.001, 0.01, 0.05, and 0.1667. The sphere radius changes periodically with time. Gravity, surface tension, and Marangoni effects are included

4.1 Scaling with respect to $R(t)$

The governing equations that describe $h(x,t)$ and $\Gamma(x,t)$ are shown in Eqs. (29) and (30). Multiplying both sides of both equations by $R^2(t)$ and combining terms allow us to write

$$\frac{\partial}{\partial t}\ln(R^2(t)h) + \frac{\partial}{\partial x}\left(R^2(t)h^2(1-x^2)\left[Q_1 h + \frac{1}{2}Q_2\right]\right) = 0, \tag{37}$$

$$\frac{\partial}{\partial t}\ln(R^2(t)\Gamma) + \frac{\partial}{\partial x}\left(R^2(t)h\Gamma(1-x^2)\left[\frac{3}{2}Q_1 h + Q_2\right]\right)$$
$$= \frac{\partial}{\partial x}\left(\mathcal{D}(1-x^2)\frac{\partial \Gamma}{\partial x}\right) + \frac{\alpha\tau R^2(t)}{\Gamma_0} - \beta\tau R^2(t)\Gamma. \tag{38}$$

With the change of dependent variables $\tilde{h}(x,t) = h(x,t)R^2(t)$ and $\tilde{\Gamma}(x,t) = \Gamma(x,t)R^2(t)$, we can rewrite these as

$$\frac{\partial \tilde{h}}{\partial t} + \frac{\partial}{\partial x}\left(\tilde{h}^2(1-x^2)\left(\left[\frac{\mathcal{G}}{R^5(t)} + \frac{\mathcal{S}}{\sqrt{2\tilde{\Gamma}}R^9(t)}\frac{\partial}{\partial x}\left(2\tilde{h} + \frac{\partial}{\partial x}\left((1-x^2)\frac{\partial \tilde{h}}{\partial x}\right)\right)\right]\tilde{h} - \frac{(2\tilde{\Gamma})^{-3/2}\mathcal{M}}{2R(t)}\frac{\partial \tilde{\Gamma}}{\partial x}\right)\right) = 0, \tag{39}$$

and

$$\frac{\partial \tilde{\Gamma}}{\partial t} + \frac{\partial}{\partial x}\left(\tilde{h}\tilde{\Gamma}(1-x^2)\left(\frac{3}{2}\left[\frac{\mathcal{G}}{R^5(t)} + \frac{\mathcal{S}}{\sqrt{2\tilde{\Gamma}}R^9(t)}\frac{\partial}{\partial x}\left(2\tilde{h} + \frac{\partial}{\partial x}\left((1-x^2)\frac{\partial \tilde{h}}{\partial x}\right)\right)\right]\tilde{h} - \frac{(2\tilde{\Gamma})^{-3/2}\mathcal{M}}{R(t)}\frac{\partial \tilde{\Gamma}}{\partial x}\right)\right)$$
$$= \frac{\partial}{\partial x}\left(\frac{\mathcal{D}}{R^2(t)}(1-x^2)\frac{\partial \tilde{\Gamma}}{\partial x}\right) + \frac{\alpha\tau R^2(t)}{\Gamma_0} - \beta\tau\tilde{\Gamma}. \tag{40}$$

We observe that these equations have the same forms as the constant-radius case, only with parameters that depend on various powers of $R(t)$. It should be noted that as $R(t)$ varies between its maximum scaled value of unity and the lower bound $1 - 2R_\mathrm{m} \approx 0.6$ (when $R_\mathrm{m} = 0.2$ as suggested earlier), factors such as R^5 and R^9 attain much smaller minimum values and change the relative importance of the effects of gravity, surface tension, Marangoni flow, surface diffusion and surfactant production rate.

When some of those effects act in isolation, a mathematical trick allows us to remove the time-dependent radius $R(t)$ from the equation by defining a new time-like variable. For instance, if we consider the problem under the effect of surface tension only, we can rewrite Eq. (39) after defining a new time-like variable $\tilde{t} = \int_0^t R^{-9}(\tau)\,\mathrm{d}\tau$, in the form

$$\frac{\partial \tilde{h}}{\partial \tilde{t}} + \frac{\partial}{\partial x}\left(\tilde{h}^2(1-x^2)\mathcal{S}\sigma(\tilde{\Gamma})\frac{\partial}{\partial x}\left(2\tilde{h} + \frac{\partial}{\partial x}\left((1-x^2)\frac{\partial \tilde{h}}{\partial x}\right)\tilde{h}\right)\right) = 0. \tag{41}$$

This equation admits $\tilde{h} \equiv 1$ as its attracting steady-state solution, which implies that $h(t) = 1/R^2(t)$ is a global attractor for Eq. (29) when only surface tension is acting; that is, non-uniform initial film profiles tend to reach the uniform state that depends only upon time and varies as the radius changes, while conserving the fluid volume.

4.2 Effect of gravity

One mathematically interesting case which can be analyzed readily using the method of characteristics is when gravity alone acts on the film, while surface tension and all surfactant effects are absent (i.e., only parameter $\mathcal{G}$ is nonzero). Upon defining the new time-like variable $\tilde{t} = \mathcal{G}\int_0^t R^{-5}(\tau)\,\mathrm{d}\tau$, Eq. (39) can be written as

$$\frac{\partial \tilde{h}}{\partial \tilde{t}} + \frac{\partial}{\partial x}(\tilde{h}^3(1-x^2)) = 0, \tag{42}$$

having the conservation form. Its expanded form reads as

$$\frac{\partial \tilde{h}}{\partial \tilde{t}} + 3\tilde{h}^2(1-x^2)\frac{\partial \tilde{h}}{\partial x} = 2x\tilde{h}^3, \tag{43}$$

which is a first-order quasilinear PDE amenable to the method of characteristics. The characteristic form of this equation is equivalent to a system of two first-order nonlinear ODEs:

$$\frac{\mathrm{d}\tilde{h}}{\mathrm{d}\tilde{t}} = 2x\tilde{h}^3 \quad \text{along paths:} \quad \frac{\mathrm{d}x}{\mathrm{d}\tilde{t}} = 3(1-x^2)\tilde{h}^2. \tag{44}$$

With a change of variable $y = \tilde{h}^{-2}$, we can rewrite the previous two equations as

$$\frac{\mathrm{d}x}{\mathrm{d}\tilde{t}} = \frac{3(1-x^2)}{y}, \quad \frac{\mathrm{d}y}{\mathrm{d}\tilde{t}} = -4x. \tag{45}$$

Upon dividing these, we find

$$\frac{\mathrm{d}y}{\mathrm{d}x} = -\frac{4xy}{3(1-x^2)}, \tag{46}$$

solution of which in terms of $\tilde{h}$ is given by

$$\tilde{h}(\tilde{t})\,(1-x(\tilde{t})^2)^{1/3} = \text{constant}. \tag{47}$$

Although the characteristics obtained from equations (44) cannot be obtained in closed form, we can make progress at the two poles. Notice that $\mathrm{d}x/\mathrm{d}t = 0$ at $x = \pm 1$, which shows that characteristics through $x = \pm 1$ are perpendicular to the x-axis. As such, we can find $h(x = \pm 1, t)$ by solving the first equation in (44)

$$\frac{\mathrm{d}\tilde{h}(\pm 1, t)}{\mathrm{d}t} = \pm 2\tilde{h}^3, \quad \tilde{h}(x, 0) = 1,$$

assuming a uniform initial profile with $h = 1$ throughout. This yields $\tilde{h}(\pm 1, t) = 1/\sqrt{1 \mp 4t}$, which shows that at the north pole, the film thickness tends to zero for long times at the rate $t^{-1/2}$, and at the south pole, the film thickness will blow up in finite time at the point $t = 0.25$. Since surface tension is a stabilizing effect, the rate of convergence to zero at the north pole when both gravity and surface tension are present will be slower than $t^{-1/2}$.

We can also integrate the characteristic equations (44) numerically starting at various initial points $-1 < x_\mathrm{o} < 1$. While the results have not been displayed here, we find that all characteristics not emanating from the north pole ultimately reach the south pole in finite time, at which time the solution diverges. The closer x_o is to the south pole, the faster the blow-up occurs, with the blow-up time approaching 0.25 as x_o tends to 1. Therefore, up to the first blow-up time of $t = 0.25$ at the south pole itself, the solution remains regular everywhere else, and the numerical solution does indeed satisfy condition (47) along the characteristics. It should be noted that this analysis applies equally to the case where the radius of the alveolus is a constant. The introduction of the time-like variable $\tilde{t}$ removes any time-dependence of radius R from the analysis.

5 Discussion and further research questions

One key observation from our numerical simulations with parameters chosen based on real experimental values is that if a small amount of surfactant is delivered into the alveolus in the form of an aerosol drop and it makes contact with the alveolar fluid layer at a point, the time it takes for it to spread uniformly over the entire interfacial area to form a monolayer is quite fast ($\approx 10^{-3}$ s) but the required time for the thin film of alveolar fluid to regain a relatively uniform thickness after the surfactant droplet deposition could be much longer (≈ 1 min).

We derived our model under the assumption that lung surfactant forms a monolayer inside the alveolar compartment, but the real structure is much more complicated. It was experimentally observed that the microscopic membrane formed by lung surfactant consists of multiple layers and can even form membrane tubes and other myelin figures [36]. These stacked interfaces with microscopic tubes and helices form a viscoelastic bulk material with near-zero surface tension which has not been studied fully and is not yet well understood. The authors of [36] came to the conclusion that lung surfactant could be modeled as a highly viscous multilayered material that supports any Laplace pressure simply by viscoelastic shear of the tightly stacked multilamellar membranes.

Also, our model did not take into account connections between multiple alveoli and the role of surfactant in the averaging of alveoli sizes. Surfactant helps all alveoli in the lung expand at nearly the same rate, since if one

expands more quickly, it will experience a rise in surface tension slowing its rate of expansion. It also means the rate of shrinking is more uniform, since if one reduces in size more quickly, its surface tension will reduce more, so the other alveoli can contract more easily and catch up to it. Surfactant reduces surface tension more readily when the alveoli are smaller because the surfactant is more concentrated. We plan to capture this size regulation effect of lung surfactant in our future research by modeling a multi-alveoli system.

In this connection, existing mathematical models that include an opening between the alveoli and the bronchiole are also relevant [37–39]. References [37,38] focus on the mechanisms of self-cleansing of alveoli. As the alveolus changes size and surfactants become more or less concentrated on the interface, the difference between the surface tension inside the alveolus and that in the bronchiole drives a Marangoni flow into or out of the alveolus. The authors argue that there can result a small net outflow of fluid out of the alveolus that can help remove external particles that may have entered. Reference [39] concerns alveoli that have been partially filled with liquid and shows the existence of time-averaged streaming flows within the thick fluid layer due to the presence of surfactants.

Synthetic pulmonary surfactants, which are currently administrated to prematurely born infants, differ in surface viscosity. Viscosity is believed to influence the rate, extent, and the uniformity of distribution of surfactant in the lungs. Surfactants with lower surface viscosity are preferred in neonatology for endotracheal application because they allow a more uniform and rapid distribution of the instilled surfactant with less loss due to the coating of the upper airways. Despite its widespread use, the optimal method of surfactant administration in prematurely born infants has not been clearly determined yet [40]. Several aspects of administration techniques that can influence surfactant delivery into the pulmonary airways including the bolus volume, injection rate, gravity and orientation, ventilation strategies, alveolar recruitment, and viscosity and surface tension of the fluid instilled are discussed in the review article [40].

An additional challenging topic would be to model the entire dynamics of synthetic surfactant delivery into the alveoli. From the bronchi, the dividing airways become progressively smaller with an estimated 23 divisions before ending at an alveolus. High-resolution MRI scans of the lungs and airways allow one to visualize only the first eight branches and, of these, only the first six can be reconstructed from the MRI image by 3D printing, although microCT imaging and use of hyper-polarized helium or xenon in magnetic resonance imaging is making the finer structures more accessible. As such, a fluid dynamic model is ideal for optimizing the parameters for the process of surfactant delivery into the lungs.

Acknowledgements This work was partially supported by a Grant from the Simons Foundation (#275088 to Marina Chugunova). The authors also thank the referees for their valuable comments and for bringing some references to our attention.

Appendix A: Microgravity

Another useful approach which could provide insight into the behavior of alveolar fluid in a microgravity environment is to perform a regular perturbation analysis when the gravity parameter $\mathcal{G}$ is very small but nonzero. Consider Eq. (35) in the presence of surface tension in a microgravity environment, i.e., when $\mathcal{G} = \delta \ll 1$, without considering the effects of production or degradation of surfactant. Assume that the solution h has an asymptotic expansion of the form:

$$h = h_0 + \delta h_1 + \delta^2 h_2 + \cdots \tag{48}$$

The equation that describes the leading order term h_0 is found to be

$$\frac{\partial h_0}{\partial t} + \frac{\partial}{\partial x}\left(h_0^3(1-x^2)\mathcal{S}\frac{\partial}{\partial x}\left(2h_0 + \frac{\partial}{\partial x}\left((1-x^2)\frac{\partial h_0}{\partial x}\right)\right)\right) = 0, \tag{49}$$

steady-state solution of which can be the constant $h_0 = 1$, depending on the initial condition. At the first order, the equation becomes

$$\frac{\partial h_1}{\partial t} + \frac{\partial}{\partial x}\left(h_0^3(1-x^2) + (1-x^2)\mathcal{S}\left(h_0^3\frac{\partial}{\partial x}\left(2h_1 + \frac{\partial}{\partial x}\left((1-x^2)\frac{\partial h_1}{\partial x}\right)\right)\right.\right.$$
$$\left.\left. + 3h_0^2 h_1\frac{\partial}{\partial x}\left(2h_0 + \frac{\partial}{\partial x}\left((1-x^2)\frac{\partial h_0}{\partial x}\right)\right)\right)\right) = 0,$$

steady-state solution of which corresponding to the state $h_0 = 1$ satisfies

$$\frac{\partial}{\partial x}\left((1-x^2) + (1-x^2)\mathcal{S}\frac{\partial}{\partial x}\left(2h_1 + \frac{\partial}{\partial x}\left((1-x^2)\frac{\partial h_1}{\partial x}\right)\right)\right) = 0. \tag{50}$$

The general solution of this fourth-order equation can be written as

$$h_1 = C_1 + C_2 x + \frac{1}{12\mathcal{S}}[-4x - \ln(1-x)(3 - 2x + 3\mathcal{S}(C_3 x + C_4))$$
$$+ \ln(1+x)((2x+3) + 3\mathcal{S}(C_3 x + C_4))].$$

This solution indicates that one cannot simultaneously remove the logarithmic singularities at $x = 1$ and -1 through any choice of constants C_3 and C_4. This suggests that obtaining a steady equilibrium shape without dry zones or touchdown points on the surface may not be possible when gravity is present (however small).

References

1. Matthay MA, Folkesson HG, Clerici C (2002) Lung epithelial fluid transport and the resolution of pulmonary edema. Physiol Rev 82(3):569–600
2. Shier D, Butler J, Lewis R (2007) Human anatomy and physiology. McGraw-Hill, Boston
3. Mason RJ (2006) Biology of alveolar type II cells. Respirology 11(Suppl):S12–S15
4. West JB, Elliott AR, Guy HJ, Prisk GK (1997) Pulmonary function in space. JAMA 277(24):1957–1961
5. Bryndina I, Vasilieva N (2014) Effects of simulated microgravity on surfactant and water balance of lung in animals with different resistance to stress. In: 40th COSPAR Scientific Assembly, 2–10 August 2014, Moscow, Russia, Abstract F4.4-17-14
6. Williams MC, Cao Y, Hinds A, Rishi AK, Wetterwald A (1996) T1 alpha protein is developmentally regulated and expressed by alveolar type I cells, choroid plexus, and ciliary epithelia of adult rats. Am J Respir Cell Mol Biol 14(6):577–585
7. Verkman AS, Matthay MA, Song Y (2000) Aquaporin water channels and lung physiology. Am J Physiol Lung Cell Mol Physiol 278(5):L867–L879
8. Crapo JD, Young SL, Fram EK, Pinkerton KE, Barry BE, Crapo RO (1983) Morphometric characteristics of cells in the alveolar region of mammalian lungs. Am Rev Respir Dis 128(2P2):S42–S46
9. Haies DM, Gil J, Weibel ER (1981) Morphometric study of rat lung cells. I. Numerical and dimensional characteristics of parenchymal cell population. Am Rev Respir Dis 123(5):533–541
10. Carnielli VP, Zimmermann LJ, Hamvas A, Cogo PE (2009) Pulmonary surfactant kinetics of the newborn infant: novel insights from studies with stable isotopes. J Perinatol 29:S29–S37
11. Notter RH, Gupta R, Schwan AL, Wang Z, Shkoor MG, Walther FJ (2016) Synthetic lung surfactants containing SP-B and SP-C peptides plus novel phospholipase-resistant lipids or glycerophospholipids. PeerJ 4:e2635
12. Fehrenbach H (2001) Alveolar epithelial type II cell: defender of the alveolus revisited. Respir Res 2(1):33
13. Castranova V, Rabovsky J, Tucker JH, Miles PR (1988) The alveolar type II epithelial cell: a multifunctional pneumocyte. Toxicol Appl Pharmacol 93(3):472–483
14. Warren NJ, Tawhai MH, Crampin EJ (2009) A mathematical model of calcium-induced fluid secretion in airway epithelium. J Theor Biol 259(4):837–849
15. Walther FJ, Hernandez-Juviel JM, Waring AJ (2014) Aerosol delivery of synthetic lung surfactant. PeerJ 2:e403
16. Halpern D, Jensen OE, Grotberg JB (1998) A theoretical study of surfactant and liquid delivery into the lung. J Appl Physiol 85:333–352
17. Halpern D, Fujioka H, Takayama S, Grotberg JB (2008) Liquid and surfactant delivery into pulmonary airways. Respir Physiol Neurobiol 163:222–231
18. Taranets RM (2017) Strong solutions of the thin film equation in spherical geometry. https://arxiv.org/pdf/1709.10496
19. Kang D, Sangsawang N, Zhang G (2016) Weak solution of a doubly degenerate parabolic equation. https://arxiv.org/pdf/1610.06303

20. Jensen OE, Grotberg JB (1992) Insoluble surfactant spreading on a thin viscous film: shock evolution and film rupture. J Fluid Mech 240:259–288
21. Gaver DP, Grotberg JB (1990) The dynamics of a localized surfactant on a thin film. J Fluid Mech 213:127–148
22. Chugunova M, King JR, Taranets R (2017) The interface dynamics of a surfactant drop on a thin viscous film. Eur J Appl Math 28(4):656–686
23. Chugunova M, Taranets R (2013) Nonnegative weak solutions for a degenerate system modelling the spreading of surfactant on thin films. Appl Math Res Express 1:102–126
24. Venables JA (2000) Introduction to surface and thin film processes. Cambridge University Press, Cambridge
25. Escher J, Hillairet M, Laurençot P, Walker C (2011) Global weak solutions for a degenerate parabolic system modeling the spreading of insoluble surfactant. Indiana Univ Math J 60:1975–2019
26. Escher J, Hillairet M, Laurençot P, Walker C (2012) Thin film equations with soluble surfactant and gravity: modeling and stability of steady states. Math Nachr 285(2–3):210–222
27. Garcke H, Wieland S (2006) Surfactant spreading on thin viscous films: nonnegative solutions of a coupled degenerate system. SIAM J Math Anal 37(6):2025–2048
28. Borgas MS, Grotberg JB (1988) Monolayer flow on a thin film. J Fluid Mech 193:151–170
29. Lucassen J, Hansen RS (1967) Damping of waves on monolayer-covered surfaces. II. Influence of bulk-to-surface diffusional interchange on ripple characteristics. J Colloid Interface Sci 23:319–328
30. Kang D, Nadim A, Chugunova M (2016) Dynamics and equilibria of thin viscous coating films on a rotating sphere. J Fluid Mech 791:495–518
31. Kang D, Nadim A, Chugunova M (2017) Marangoni effects on a thin liquid film coating a sphere with axial or radial thermal gradients. Phys Fluids 29(7):072106
32. Rausch SMK, Haberthür D, Stampanoni M, Schittny JC, Wall WA (2011) Local strain distribution in real three-dimensional alveolar geometries. Ann Biomed Eng 39(11):2835–2843
33. Nadim A (1996) A concise introduction to surface rheology with application to dilute emulsions of viscous drops. Chem Eng Commun 148–150:391–407
34. Carney DE, Bredenberg CE, Schiller HJ, Picone AL, McCann UG, Gatto LA, Bailey G, Fillinger M, Nieman GF (1999) The mechanism of lung volume change during mechanical ventilation. Am J Respir Crit Care Med 160(5):1697–1702
35. Edmonstone BD, Matar OK, Craster RV (2004) Flow of surfactant-laden thin films down an inclined plane. J Eng Math 50(2):141–156
36. Parra E, Kinoshita K, Needham D (2016) Micropipette technique study of natural and synthetic lung surfactants at the air-water interface: presence of a SP-B analog peptide promotes membrane aggregation, formation of tightly stacked lamellae, and growth of myelin figures. Langmuir 32(41):10570–10581
37. Podgórski A, Gradoń L (1993) An improved mathematical model of hydrodynamical self-cleansing of pulmonary alveoli. Ann Occup Hyg 37(4):347–366
38. Zelig D, Haber S (2002) Hydrodynamic cleansing of pulmonary alveoli. SIAM J Appl Math 63(1):195–221
39. Wei HH, Fujioka H, Hirschl RB, Grotberg JB (2005) A model of flow and surfactant transport in an oscillatory alveolus partially filled with liquid. Phys Fluid 17(3):031510
40. Nouraeyan N, Lambrinakos-Raymond A, Leone M, Sant'Anna G (2014) Surfactant administration in neonates: a review of delivery methods. Can J Respir Ther 50(3):91–95